Geo-Mar Lett (2009) 29:309–320
DOI 10.1007/s00367-009-0144-8

ORIGINAL

Core-based reconstruction of paleoenvironmental conditions in the southern Drake Passage (West Antarctica) over the last 150 ka

Ho Il Yoon · Kyu-Cheul Yoo · Young-Suk Bak · Yong Il Lee · Jae Il Lee

Received: 20 April 2009 / Accepted: 26 May 2009 / Published online: 25 June 2009

Abstract A deep-sea sediment core (GC98-06) from the southernmost Drake Passage, West Antarctica, shows late Quaternary depositional environments distinctly different from sedimentary drifts commonly found along the southwestern Pacific margin of the Drake Passage. The chronology of the core has been inferred using geochemical tracers of paleoproductivity and diatom biostratigraphy, and represents the paleoceanographic conditions in a continental rise setting during the last 150,000 years. Three dominant sediment types associated with distinct sedimentary processes have been identified using textural/compositional analyses: (1) hemipelagic mud (interglacial sediments) deposited from pelagic settling of bioclasts, meltwater plumes, and ice-rafted detritus; (2) terrigenous mud (glacial sediments) delivered by turbid meltwater plumes; and (3) massive muds marking the boundaries from interglacial to glacial periods. The succession of the sedimentary facies in core GC98-06 is interpreted to reflect temporal changes in environmental conditions prevailing on the continental rise of the southern Drake Passage in the course of successive climatic stages over the last 150 ka: from the bottom upward, these are glacial, interglacial, glaciation, glacial, and interglacial episodes. Variability in sediment flux and diatom abundance seem to have been related to changes in glacial advance, sea-ice extent, and specific sedimentary environments, collectively influenced by mid- to late Quaternary climatic changes.

H. I. Yoon · J. I. Lee
Korea Ocean Research and Development Institute,
Korea Polar Research Institute,
Songdo TP,
Incheon 406-840, Republic of Korea

H. I. Yoon
e-mail: hiyoon@kopri.re.kr

J. I. Lee
e-mail: leeji@kopri.re.kr

K.-C. Yoo (✉) · Y. I. Lee
School of Earth and Environmental Sciences,
Seoul National University,
Seoul 151-747, Republic of Korea
e-mail: kcyoo@kopri.re.kr

Y. I. Lee
e-mail: lee2602@snu.ac.kr

Y.-S. Bak
Department of Earth and Environmental Sciences,
Chonbuk National University,
Jeonju 561-751, Republic of Korea
e-mail: sydin@chonbuk.ac.kr

Introduction

Over the past 50 years, the western Antarctic Peninsula (WAP) has experienced rapid regional warming (Vaughan et al. 2001; Quayle et al. 2002). Given the apparent sensitive nature of this region to climate change, the establishment of detailed paleoclimatic records will enhance our ability to tie the regional climate changes to other global climate phenomena. Antarctic marine sediments have great potential to provide important data for paleoenvironmental reconstructions, in particular high-quality records of both local and regional climate change, thereby helping to understand the polar ocean climate as a whole.

Since the mid-1980s, many studies have dealt with biogenic and glaciomarine sedimentation in the WAP region (e.g., Griffith and Anderson 1989; Domack and Williams 1990; Harden et al. 1992; Domack et al. 2001; Lucchi et al. 2002; Yoon et al. 2002; Bae et al. 2003).

However, paleoclimatic records for the Drake Passage have rarely been reported in the international literature. Probably due to the thin sediment cover in the passage, only few studies have dealt with past climate/ocean variability in the Drake Passage on the basis of core data covering the late Quaternary period.

In this paper, we investigate a gravity core (GC98-06) collected near the South Shetland Trench located north of the South Shetland Islands (SSIs), our aim being to identify and interpret the mid-late Quaternary paleoceanographic conditions prevailing in the southern sector of the Drake Passage (Fig. 1), a 640-km-wide passage between the southern tip of South America and the SSIs located off the Antarctic Peninsula. The deposits on the continental rise in the Drake Passage may provide constraints on the extent and timing of glaciations on the shelf. Despite a detailed understanding of sedimentary processes and the glacial history in the WAP region (e.g., Pudsey 2000; Lucchi et al. 2002), it is still uncertain how these varied in response to paleoclimatic changes in the southern Drake Passage.

The objectives of this paper, therefore, are to determine the sedimentary facies and processes characterizing the southern Drake Passage on the basis of the evidence contained in a sediment core, and to establish links between this environmental record and associated paleoclimate changes in the course of the glacial history of the western Antarctic Peninsula region.

Physical setting

The Southern Ocean plays a key role in the global climate system by distributing large quantities of heat, salt, and freshwater via the Antarctic Circumpolar Current (ACC). The ACC flows eastward around Antarctica, providing a deep linkage to other world ocean basins (Foldvik and Gammelsrød 1988; Ganachaud and Wunsch 2000). The boundaries of the ACC are generally defined by zonal variations in specific water properties of the Southern Ocean. There are three deep-reaching fronts and three zones associated with the ACC: from north to south, the

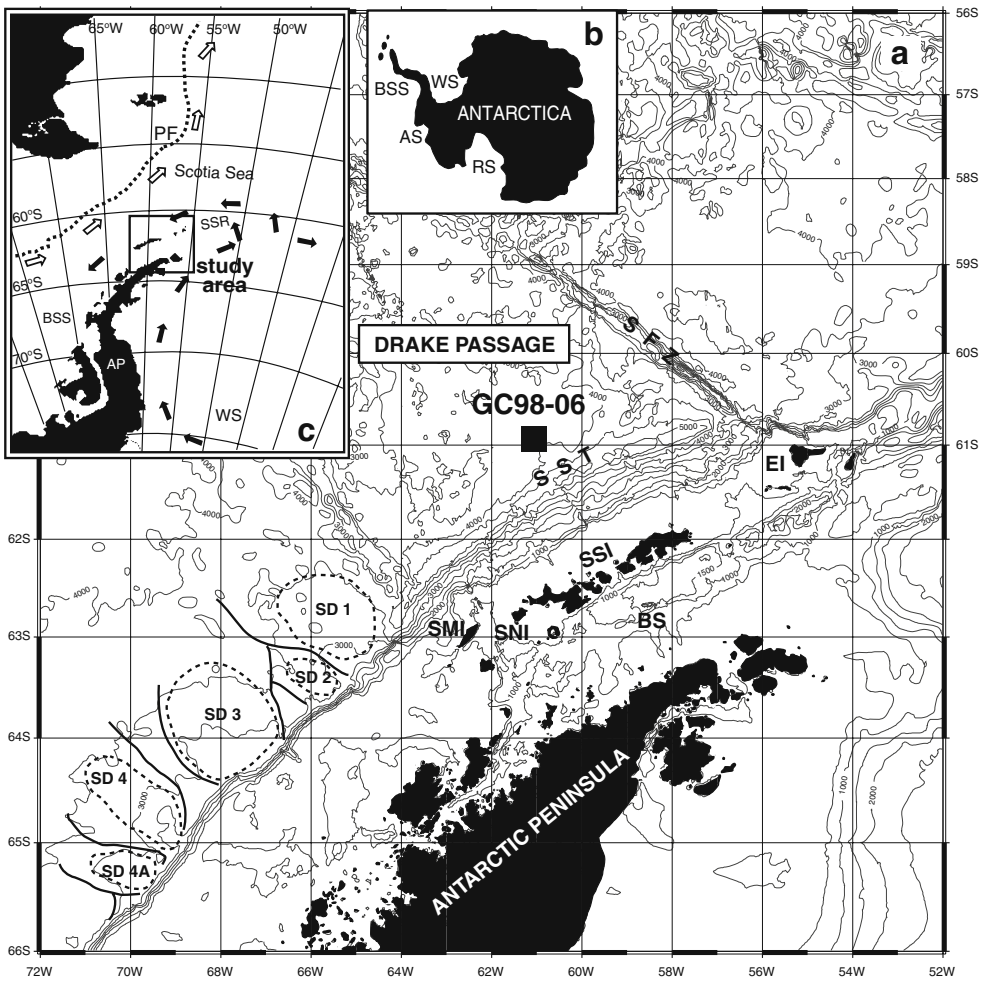

Fig. 1 **a** Bathymetry, and location of gravity core GC98-06 in the Drake Passage. Contour interval is 500 m. The *dashed lines* represent sediment drifts (*SD*), and the *thick lines* channel systems along the western Antarctic Peninsula. *BS* Bransfield Strait, *EI* Elephant Island, *SFZ* Shackleton Fracture Zone, *SSI* South Shetland Islands, *SST* South Shetland Trench, *SMI* Smith Island, *SNI* Snow Island. **b** Antarctic continent and main seas. *AS* Amundsen Sea, *BSS* Bellingshausen Sea, *RS* Ross Sea, *WS* Weddell Sea. **c** Ocean circulation systems around the Antarctic Peninsula (*AP*) and the South Shetland Ridge (*SSR*). Note the Antarctic Circumpolar Current (*open arrows*) axis along the Polar Front (*PF*, *dashed line*). The *closed arrows* represent the Antarctic Deep Water and Weddell Gyre

Subantarctic Zone, the Subantarctic Front, the Polar Frontal Zone, the Polar Front, the Antarctic Zone, and the southern ACC Front (Orsi et al. 1995).

The Drake Passage is located at 56~60°S, and provides an important pathway for the unimpeded flow of the ACC. The typical water mass consists of five main components (Naveira Garabato et al. 2002a): the Antarctic Surface Water, Upper Circumpolar Deep Water, Lower Circumpolar Deep Water, Southeast Pacific Deep Water, and Weddell Sea Deep Water. Up to 70% of the Antarctic Bottom Water forms in the Weddell Sea, and Weddell Sea Deep Water constitutes the densest water mass in the passage (Carmack 1977; Orsi et al. 1999; Naveira Garabato et al. 2002b). Bottom water of Antarctic source flows into the basins of the western Atlantic Ocean as far as 35°N, and is modified by mixing with overlying water masses. Drift sediments along the Pacific margin of the Antarctic Peninsula have been interpreted as contourites that were deposited under the influence of the most important current in the area, the ACC (Hernández-Molina et al. 2006). Although there are bottom currents flowing along the South Shetland Trench (Nowlin and Zenk 1988), there is no evidence of large sedimentary drifts in the vicinity of the study area (Kim et al. 1995).

A major morphological and structural feature of the seafloor that crosses the passage is the Shackleton Fracture Zone, an active transpressive fault zone (Klepeis and Lawver 1996). Active, albeit slow, subduction is still continuing beneath the SSIs along the South Shetland Trench. The Shackleton Fracture Zone is probably being subducted at present beneath the northern margin of the South Shetland continental block (Pelayo and Wiens 1989). A sedimentary cover is generally absent over the oceanic crust in the central Drake Passage (Maldonado et al. 2006). Today, glaciers are commonly grounded on the coast of the northern SSIs, although most continental shelf areas of the WAP region have only seasonal sea-ice cover.

Materials and methods

Core collection, radiography, grain-size analysis

The 248-cm-long gravity core GC98-06 was obtained at ~4,000 m water depth north of the South Shetland Trench (61°07.3′S, 61°01.2′W; Fig. 1). There was little disturbance and loss of surface sediments (<1 cm) during the coring operation, as indicated by intact bioturbation at the core top. The core was cut lengthwise in the ship's laboratory; one half being visually described before being sliced into 1-cm-thick, 30-cm-long slabs for X-radiography. This core half also served for measurements of magnetic susceptibility. The other half of the core was subsampled for grain-size and other analyses (see below).

Grain-size distributions of the −4.0 to +4.0 φ (16.0 mm to 0.063 mm) size fractions were determined by dry sieving of subsamples taken at 5-cm intervals. Finer fractions (4.0 φ to 11.0 φ, or 63 μm to 0.5 μm) were analyzed by means of a Micrometrics SediGraph 5000D. Computer processing of the raw data was performed after Jones et al. (1988), and sediment classification after Folk and Ward (1957). Relative granule abundances were assessed by examination of the X-radiographs (*granule* 2–4 mm fraction).

Magnetic susceptibility and radiocarbon dating

Magnetic susceptibility (MS) was measured at 1-cm intervals using a Bartington MS-2B core sensor on the split core surface. Volume MS was recorded as the dimensionless ratio between the induced magnetic field and the applied field, expressed in 10^{-7} (SI) units.

There were no calcareous microfossils suitable for age datings in the core. We used five diatomaceous bulk sediment samples for radiocarbon AMS dating, performed at the Nuclear and Geoscience Laboratory, Lower Hutt, New Zealand.

Geochemical and diatom analyses

Freeze-dried subsamples (of the bulk sediment) were ground by means of a planetary ball mill, and total carbon (TC) contents measured with a Carlo-Erba NA-1500 Elemental Analyzer (precision: ±0.4%). Total inorganic carbon (TIC) content was determined by means of a UIC model CM 5130 (precision: ±0.1%). Total organic carbon (TOC) content was obtained as the difference between TC and TIC.

Major and trace element composition was determined on bulk sediment samples using an ICP-MS Elan 6100 (Perkin Elmer Sciex) at the Geoscience Analytical Laboratory, Korea Polar Research Institute, Incheon. As not every 4-cm subsample was suitable for analysis, the data intervals vary between 4 cm and 16 cm. Selected datasets reported in this paper are for Ba, Al, U, Cd, Ni, and Zn. Ba_{bio} refers to biogenic barium.

Data on diatom assemblages were extracted from Bak et al. (2002). Because this publication is in Korean, a brief description of the methodology is given here. Bulk sediment subsamples were collected at 4-cm intervals, the carbonates and organic matter removed by reacting with 25 ml 10% hydrochloric acid and 25 ml 30% hydrogen peroxide at 100°C, and the material then washed in distilled water and centrifuged. The slide preparation was after Battarbee (1973). Per slide, at least 400 valves were counted, and (wherever possible) identified at 1,000× magnification using a Nikon E400 microscope.

Results

Lithostratigraphy, and magnetic susceptibility

The sediments of core GC98-06 are largely fine-grained, with rare evidence of lamination (Fig. 2). There are at least some signs of bioturbation throughout the core, except for a 25-cm-long section between 123 cm and 148 cm core depth, which is completely structureless. Burrows are particularly abundant in the upper part of the core (0~35 cm). Down-core granule abundances are unrelated to any of the other parameters.

Clay contents generally exceed 80%, the down-core trend being interrupted by spikes of lower values where the samples contain appreciable amounts of sand, i.e., at 5 cm and 40 cm, between 165 cm and 210 cm, and near the bottom of the core at 245 cm (Fig. 3). This is accompanied by corresponding trends in sand contents, mean grain size, and sorting. The trend of silt content, by contrast, mirror-images that of the clay content, the only departures occurring where sand is present in the samples. Significantly, the silts are the only sedimentary component that exhibits a trend similar to that of MS. For the core as a whole, MS values range between 24 and 255.

The core can be subdivided into five lithofacies based on sediment color, magnetic susceptibility, relative granule abundance, and silt content (Fig. 3): from the core top downward, these are units I, II, III, IV, and V. Unit I occupies the upper 36 cm of the core, and comprises strongly bioturbated, olive gray to greenish-gray diatomaceous clayey mud. MS values progressively increase from 84 at the top, to 153 at 36 cm. This trend is similar to that of the silt contents, which increase from ~12% at the top to ~15% at 35 cm. Clay contents follow an opposite trend, gradually decreasing from 88 to 85%, the only exception being a downward spike at 5 cm where, due to a sand content of ~7%, a lower value is recorded (~82%). Granule abundance reaches a peak value of 61 at 9 cm from the top. The sediment is generally poorly sorted (1.8 φ), with a mean grain size of 10.7 φ, except at 5 cm core depth where, due to the presence of sand, it is slightly coarser (mean grain size of 10 φ) and very poorly sorted (~3 φ). Most of unit I is crisscrossed by planolites, i.e., a meandering type of trace fossil probably representing the feeding burrow of a worm-like animal; a few halo burrows reach 2 cm in diameter (Fig. 2).

Unit II, at 36~124 cm core depth, consists of slightly bioturbated (faint burrow traces), dark gray to dark greenish-gray diatomaceous silty mud (Fig. 2). Compared to the other units, silt contents are relatively high at 13~17 wt%. The lower values are found at the top, in the

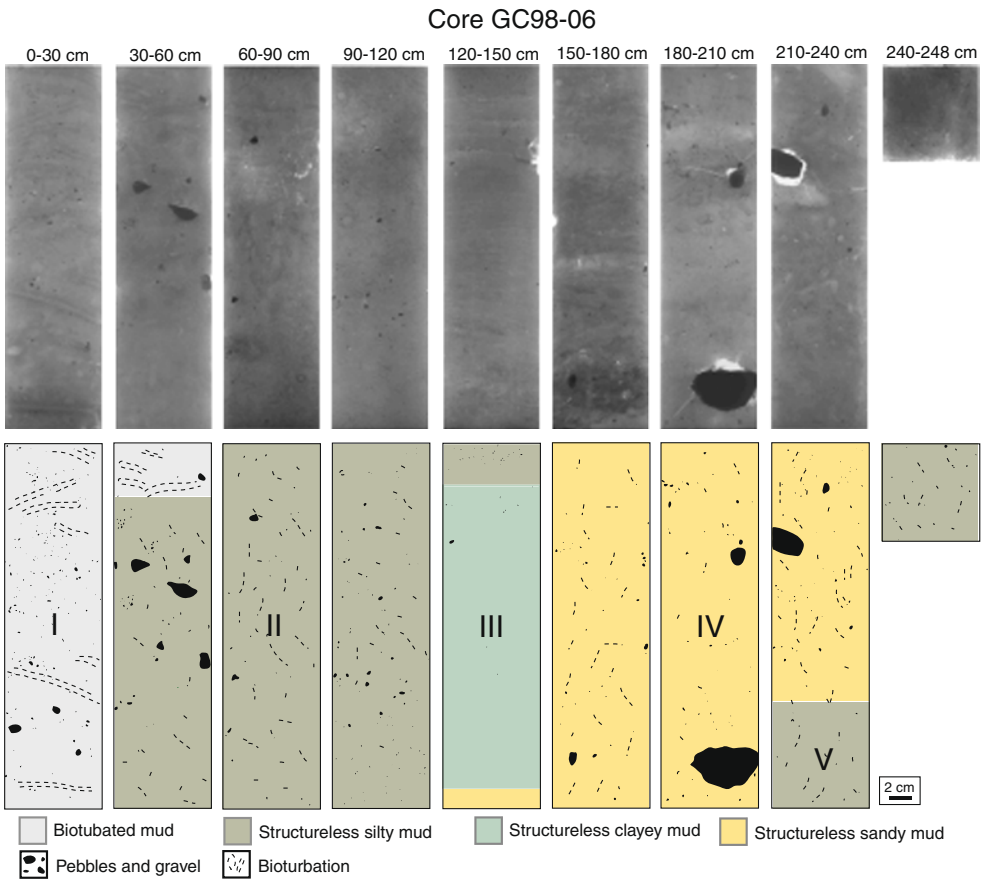

Fig. 2 X-radiographs of core GC98-06 (*top*) with corresponding lithological logs (*bottom*) highlighting units I to V by different shadings. Note that the core sediments are largely fine-grained, with rare evidence of lamination

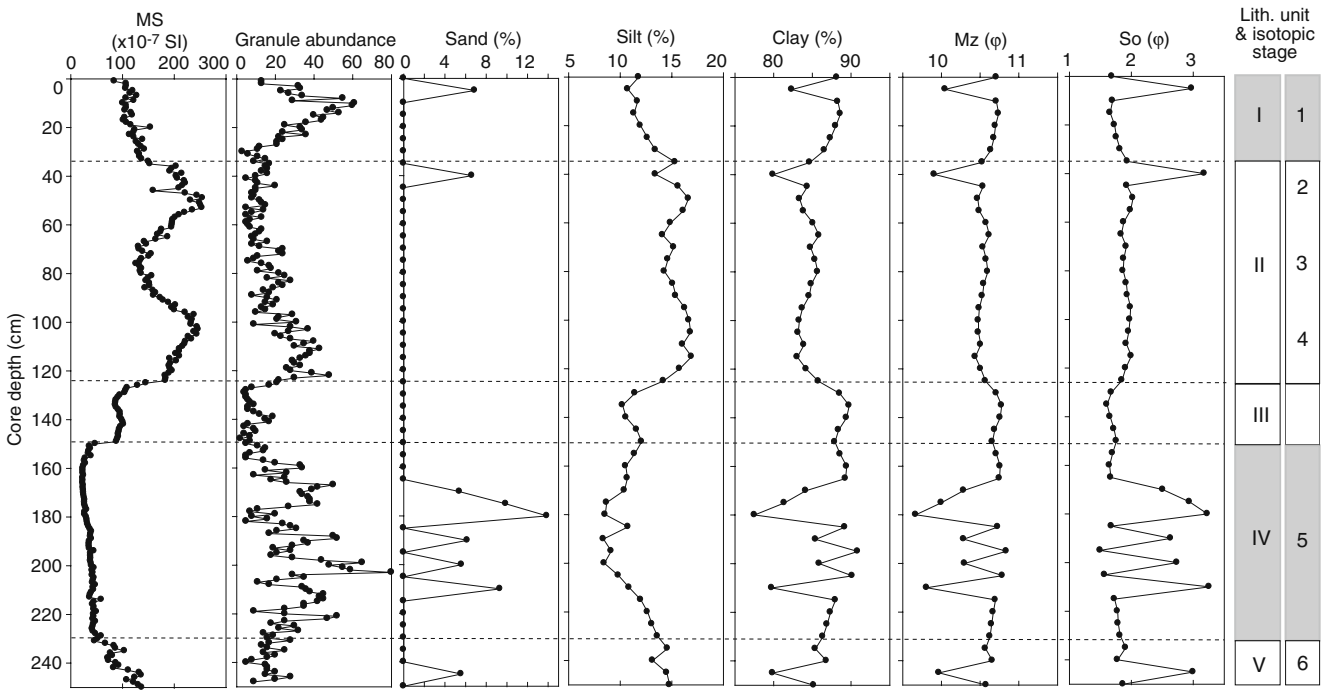

Fig. 3 Down-core variations in magnetic susceptibility (*MS*, $\times 10^{-7}$ SI), relative granule abundance, sand, silt and clay contents (dry wt% of bulk sediments; *clay* <4 μm fraction), mean grain size (*Mz*, φ), and sorting (*So*, φ) for core GC98-06. The *shading* highlights the marine isotopic stages of the present (Holocene, MIS 1) and the penultimate (Eemian, MIS 5) interglacial periods

middle, and at the bottom of the unit. The trend is similar for MS, which reaches the highest down-core values in this unit (255 in the upper, and 247 in the lower peak, respectively). Unit II is devoid of sand, except at 40 cm core depth where the sand content is nearly 7%. As a consequence, the mean grain size (~9.9 φ) here is coarser than elsewhere in unit II. Correspondingly, the clay content (~80%) is relatively low, and the sorting is poorer (3.2 φ), contrasting with the otherwise uniform trends for unit II as a whole (clay contents of ~86%, sorting of ~2 φ, mean grain sizes of ~10.5 φ). Based on relative granule abundance (Fig. 3) and degree of clustering (Fig. 2), unit II can be divided into two subfacies: (1) an upper one from 36~64 cm core depth, consisting of almost structureless silty mud with a lower abundance of granules (<20), these being more clustered, and (2) a lower one from 64~124 cm core depth, also consisting of almost structureless silty mud, but with a higher abundance of granules (<48), these being more dispersed.

Unit III, between 124 cm and 148 cm core depth, shows gray diatomaceous, completely structureless massive mud with no bioturbation, and only sparse granules. Silt and clay contents vary from 10–14% and 86–88%, respectively. Mean grain size is ~10.7 φ, and sorting ~1.8 φ.

Unit IV, between 148 cm and 230 cm core depth, comprises moderately bioturbated, gray to dark gray diatomaceous, almost structureless sandy mud with faint burrow traces (Fig. 2). The middle part of this unit, at 160~214 cm core depth, shows strong fluctuations in sand content, with a maximum value of ~14%. This noisy pattern is mirrored in the clay content (80~90%), the mean grain size (9.6 to 10.7 φ) and sorting (2~3 φ), as well as the relative granule abundance (5~52; Fig. 3). The trend described by the silt content is, by contrast, much more uniform, decreasing from ~12% at the top to ~8% in the middle, and thereafter increasing progressively to ~15% at the base of the unit. Unit IV is the only facies in which the MS trend is less well correlated with that of the silt content, being more subdued than in other parts of the core.

The lowermost unit V, the total thickness of which is unknown, extends from 230 cm to the bottom of the core at 248 cm. It comprises slightly bioturbated, dark gray structureless diatomaceous silty mud, with some faint burrow traces. Of the four samples characterizing this unit, one contains ~5% sand, the spike being faithfully recorded in the trends of the clay content, mean grain size and sorting, but not in the silt content, the latter being again well correlated with MS. Relative granule abundance fluctuates around a mean value of ~15.

TOC, and trace elements

For the core as a whole, TOC content is mostly very low (<0.3%), but its distribution is markedly cyclical, with peaks in units I and IV (Fig. 4). With the exception of samples containing sand, the down-core trend of TOC is

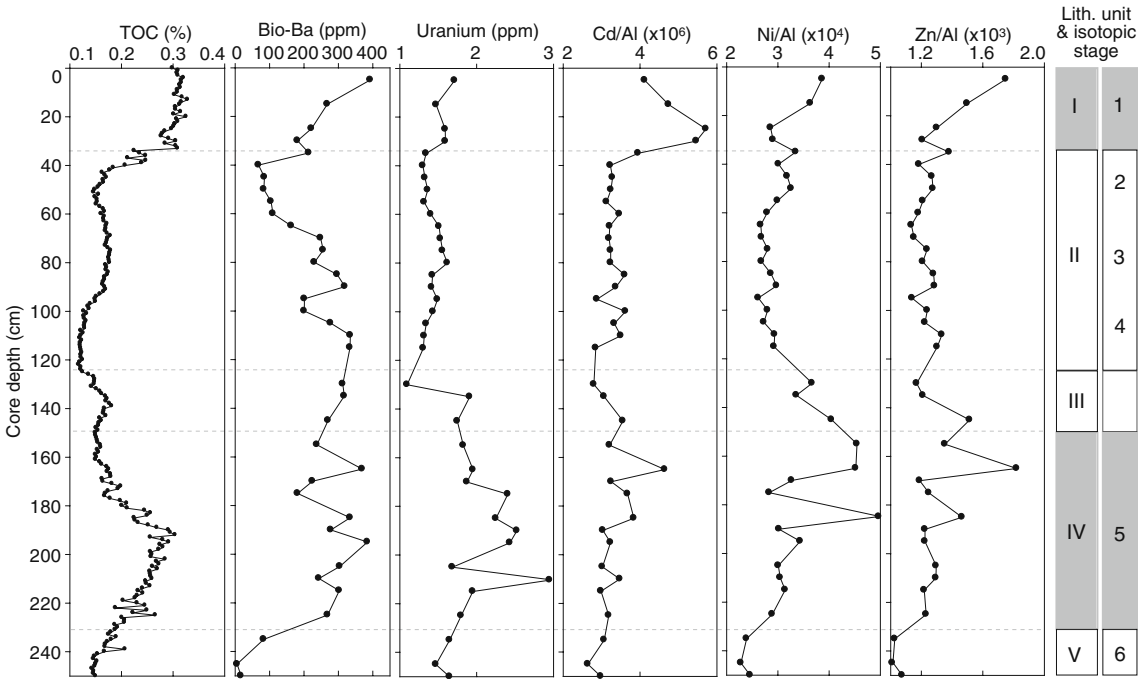

Fig. 4 Down-core variations in total organic carbon (*TOC*, dry wt%), biogenic Ba (ppm), and U (ppm), as well as Al-normalized trace element ratios (Cd/Al, Ni/Al, and Zn/Al) for core GC98-06. *Shading* as in Fig. 3

faintly positively correlated with clay, and negatively with silt content (cf. Fig. 3). None of the trace elements are correlated with TOC or any of the textural sediment parameters. On the other hand, uranium, Ni/Al, and Zn/Al are more or less positively correlated with each other, whereas Ba_{bio} and Cd/Al show no correlation with any of the other trace elements (Fig. 4).

AMS ^{14}C dating

In the absence of datable carbonate tests, altogether five AMS ^{14}C age datings were carried out on bulk sample material consisting of diatomaceous mud (Table 1). The uncorrected radiocarbon ages consistently increase down-core from 12,864±60 years B.P. at the surface, to 17,997± 90 years B.P. at a depth of 10 cm, 21,580±140 years B.P. at 125 cm, 24,360±190 years B.P. at 150 cm, and 29,420± 280 years B.P. at 230 cm. If these dates are correct, then the core represents a period of about 16.5 ka (uncalibrated) of the latest Pleistocene, with average down-core sedimentation rates of 1.90, 32.10, 8.99, and 15.81 cm/1,000 years, respectively (mean for whole core: 13.89 cm/1,000 years). As will be shown in the Discussion, there are good reasons to doubt the accuracy of these dates, and to suspect that an age span of 150 ka is more likely, in the light of results obtained by other investigations reasonably close to the location of core GC98-06.

Diatom assemblages

A total of 64 species belonging to 23 genera of diatoms were identified in the samples from the core (cf. Bak et al. 2002). Valve abundance (Fig. 5) increases sharply from almost zero at the top of the core, to 6 ($\times 10^7$) in the middle part of unit I, before decreasing again to almost zero in the upper part of unit II. From here, the abundance gradually increases through unit II, and up to the upper part of unit III ($\sim 2 \times 10^7$), where it begins to fluctuate strongly between

Table 1 AMS ^{14}C dating of bulk sediments, and corresponding lithofacies of core GC98-06

Core depth (cm)	Age (uncorrected) (^{14}C years B.P.)	Lithofacies	Lab. code
0	12,864±60	Diatomaceous mud	NZA16305
10	17,997±90	Diatomaceous mud	NZA16306
125	21,580±140	Diatomaceous mud	NZA16297
150	24,360±190	Diatomaceous mud	NZA16298
230	29,420±280	Diatomaceous mud>	NZA16307

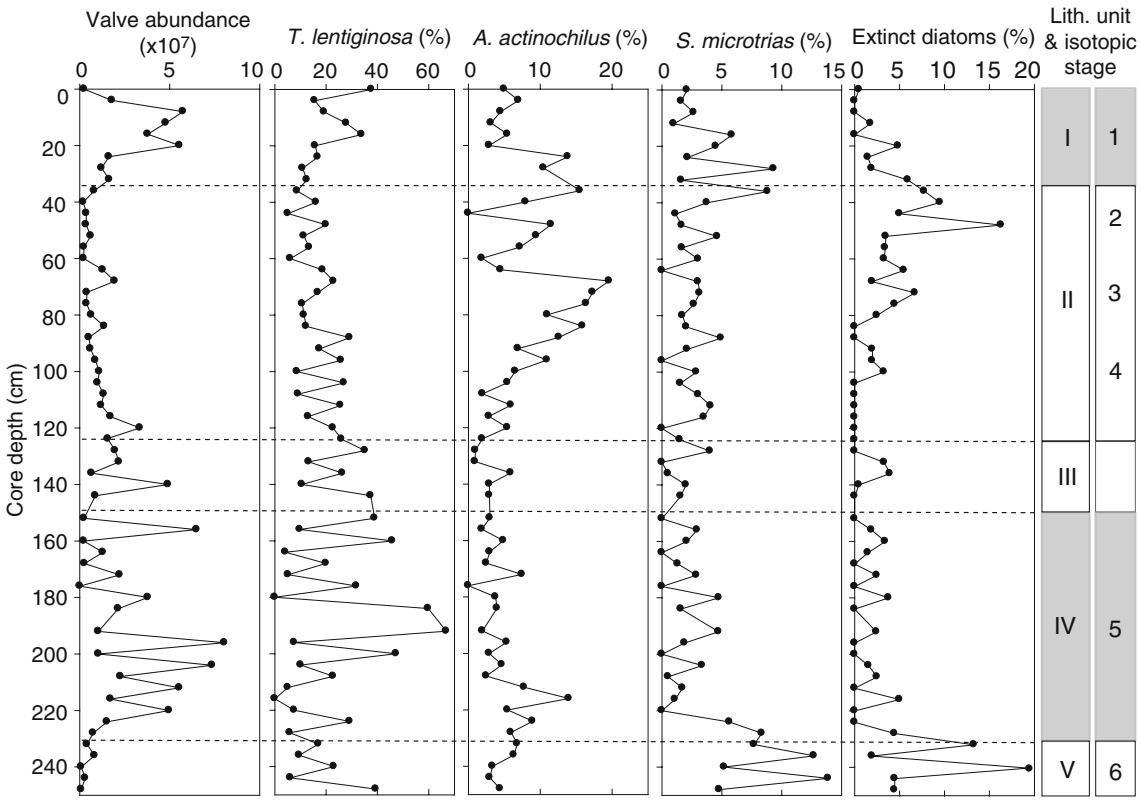

Fig. 5 Diatom analyses of core GC98-06, showing down-core variations in valve abundance ($\times 10^7$), and in the relative abundance (% of total counts) of *Thalassiosira lentiginosa*, *Actinocyclus actinochilus*, *Stellarima microtrias*, as well as the extinct diatoms *Actinocyclus ingens* and *Stephanopyxis* spp. (after Bak et al. 2002). *Shading* as in Fig. 3

very low values and maximum counts of up to 8 ($\times 10^7$) in unit IV. Toward the base of unit IV, the abundance begins to decrease almost uniformly to once again reach very low values at the bottom of the core.

In Fig. 5, the down-core trends of the diatom species *Thalassiosira lentiginosa*, *Actinocyclus actinochilus*, *Stellarima microtrias*, as well as some extinct diatoms are illustrated. Of these, only *S. microtrias* and the extinct diatoms show some degree of down-core correlation. No correlation exists with any of the sedimentary parameters or trace element data.

In general, *A. actinochilus*, one of the representative sea-ice diatoms, has a minimum relative abundance of less than 5% in unit IV, and *S. microtrias* shows high abundance in unit V. The extinct diatom species *Actinocyclus ingens* and *Stephanopyxis* spp., abundant during the early Pliocene and which no longer inhabit Antarctic waters, are also present in the core, their abundance oscillating down-core between <5% in units I and IV, and >5% in the upper parts of units II and V. In units II and III, the diatom content is low, and the assemblage is poorly preserved, showing signs of reworking (e.g., the lower Pleistocene form *A. ingens* and *Stephanopyxis* spp.). Down-core numbers of two reworked diatom species (*Denticulopsis dimorpha* and *Denticulopsis hustedtii*) in about 200 counts per sample are listed in Table 2.

Discussion

Chronology

The AMS ^{14}C age at the top of the core was determined to be 12,864±60 years B.P. (Table 1). This age is much older than the general age range based on the accepted ocean reservoir correction for Antarctica (1,200~1,400 years; Berkman et al. 1998), or on the reservoir correction for the Antarctic Peninsula continental shelf (e.g., ~9,000 years B.P.; Yoon et al. 2002). Considering the absence of erosional features, we exclude any loss of core-top material during coring and/or earlier reworking events. This anomalous old age may therefore be explained either by the low TOC content (<0.3%), or more likely, by the presence of reworked older carbon. In addition to the extinct diatoms described above, also the Miocene and Pliocene diatoms *D. dimorpha* and *D. hustedtii*, which occur ubiquitously in the core sediment (Table 2), mitigate against a younger age. This questions the reliability of all the AMS ^{14}C ages

Table 2 Down-core occurrence of the diatom species *Denticulopsis dimorpha* and *Denticulopsis hustedtii* per about 200 diatoms in core GC98-06 (after Bak et al. 2002)

Core depth interval (cm)	*Denticulopsis dimorpha*[a]	*Denticulopsis hustedtii*[b]
0–16	1	0
16–32	2	0
32–48	2	2
48–64	2	3
64–80	4	9
80–96	0	4
96–112	0	2
112–128	0	1
128–144	1	2
144–160	0	4
160–176	2	10
176–192	2	0
192–208	0	2
208–224	0	2
224–248	2	0

[a] Last occurrence: 4.5 Ma (early Pliocene; Ciesielski 1983)

[b] Last common occurrence: 10.1 Ma (late Miocene; Baldauf and Barron 1991)

obtained from bulk sediment samples of core GC98-06. For this reason, the establishment of a chronostratigraphic framework for the core was not attempted. However, the maximum depositional age can be inferred from the absence of the extinct diatom *Hemidiscus karstenii* in the core. This implies that the age of this core can at most extend to MIS 6, considering that Gersonde and Barcena (1998) documented the last appearance of *H. karstenii* in the sub-Antarctic region at ~191,000 years B.P.

With this maximum possible depositional age at hand, the chronology of the core was estimated qualitatively in terms of the variations in magnetic susceptibility, biogenic barium, and diatom assemblage. Ba_{bio} has, for example, been successfully used as a paleoproductivity indicator by Pudsey and Howe (1998). In Quaternary cores from the Weddell and Scotia seas, adjacent to the Drake Passage, Ba_{bio} levels are consistently high during the warm marine isotope stages (MISs) 1 and 5, and low during the cold stages 2 to 4, and 6 (Bonn 1995). On the basis of distinctive down-core peaks and troughs in Ba_{bio} enrichment, it was therefore possible to confidently delineate the climatic stages of the core. Units I and IV thus correspond to interglacial isotope stages 1 and 5, respectively, and unit II to glacial stages 2 to 4 (Fig. 4). The bottommost part of the core (unit V) is characterized by abrupt decreases in Ba_{bio} content and trace element ratios, which is suggestive of MIS 6 sediments. Unit III matches well with the interglacial to glacial (G) transitional facies, according to the stratigraphic framework developed by Pudsey and Camerlenghi (1998), and Pudsey (2000) for the western Antarctic Peninsula region. The glacial to interglacial (IG) transitional facies is characterized by the coexistence of typical glacial and interglacial features in the WAP region (Lucchi et al. 2002), but such an IG transition was not clearly observed in the present core.

Sedimentary processes

Interglacial sediments

During interglacials, grounded glacier termini retreated to the vicinity of the present coastline. Sediment released in freshwater plumes from the coastline is generally trapped on the continental shelf of the WAP region to form 'plumite' facies, which show repeated alternations of about 2-cm-thick layers of coarser sediments and laminated/burrowed finer clay (Hesse et al. 1997). On the outer self, interglacial sediments are derived from a combination of pelagic settling (mainly diatoms), and settling of unsorted terrigenous sediments via wind/icebergs (Hesse et al. 1999; Lucchi et al. 2002). The area where core GC98-06 was taken is rather far from the coastline of the northern SSIs (Fig. 1), and the absence of plumite facies, and the rare occurrence of ice-rafted debris (IRD) layers in interglacial sediments imply negligible input of coarse sediments transported by turbidity currents and sediment-laden meltwater plumes related to ice-margin processes (Lucchi et al. 2002).

Strong bioturbation in unit I sediments (the Holocene) suggests a low-energy environment promoting benthos activity (Fig. 2). Moreover, Pudsey (2000) reported that, on the continental rise west of the Antarctic Peninsula, interglacial sedimentation rates ranged from 1.1 to 4.3 cm/1,000 years, and glacial sedimentation rates from 1.8 to 13.5 cm/1,000 years. Slow accumulation rates and abundant food supply would lead to bioturbation by deep-sea

benthos. In addition, the absence of laminations, coarse-grained turbidites with erosive bases and grading, and bioturbated sediments with sand/gravelly mud layers excludes the possibility of sediment reworking by strong contour and turbidity currents. This suggests that unit I represents the present interglacial period (Holocene).

The sedimentary character of unit IV suggests another, older interglacial stage. It is characterized by hemipelagic mud containing only slightly higher percentages of sand (6~14%) and silt than the terrigenous mud of the present interglacial (unit I; Fig. 3). Although iceberg drift from the study area is negligible in the Holocene, such coarse-grained sediment input may indicate a supply of ice-rafted debris during the previous interglacial period. The relatively high terrigenous sand content suggests a drift of icebergs further offshore during MIS 5 than takes place today. Thus, icebergs calved in the eastern Bellingshausen Sea and/or in the Amundsen Sea (the eastern Ross Sea; Fig. 1) during MIS 5 may have been entrained by the Antarctic Circumpolar Current, drifting toward the northeast along the margin of the western Antarctic Peninsula, thereby releasing sandy debris in the study area.

Glacial (MISs 2 to 4) and G transitional sediments

In the study area, the bulk sediments are composed of terrigenous mud containing 13~16% silt and >83% clay supplied during glacial periods (Fig. 3). The relatively high abundance of extinct diatoms during glacial periods, relative to interglacial periods (Fig. 5), indicates that the core sediment was affected by reworking and/or lateral transport. Based on the first and last appearance data, and the first common occurrence of biostratigraphical marker diatoms (Barker et al. 1999), the presence of extinct diatoms indicates that the reworked sediment may have had its source in 1.9~9.0 Ma old deposits.

Lucchi et al. (2002) reported that during glacials, the typical terrigenous sediments of MISs 2 to 4 in sediment drifts of the WAP region show a large variety of subfacies (laminated mud with silty layers, laminae and lenses, cross-stratified mud, laminated mud including IRD layers, sand- and gravel-enriched turbidites, etc.). Such diverse sediment types were interpreted to be a consequence of numerous interacting sedimentary processes related to various depositional environments (e.g., several troughs on the shelf, steep continental slope, deep-sea channel system). However, the glacial facies of core GC98-06 is rather simple, being dominated by very fine-grained mud (commonly, >80% clay), although the facies includes the highest silt content and some isolated dropstones (Fig. 3). This implies that the study area was not a very complicated depositional environment during the late Quaternary, because the flat seafloor and the absence of channel systems are inconsistent with a sediment drift setting along the southwestern Pacific margin of the Antarctic Peninsula (Pudsey 2000).

During glacials, grounded ice sheets advanced toward the edge of the continental shelf (Larter and Barker 1991). Under this condition, fine terrigenous sediment in the WAP region was supplied to the deep sea via ice rafting, turbidity currents, meltwater plumes, or bottom-current erosion (Lucchi et al. 2002). The northern SSIs continental slope is relatively gentle (Fig. 1), suggesting the possible absence of suspension clouds commonly ejected at the base of very steep slopes (Pudsey and Camerlenghi 1998). The absence of graded silt layers (laminae and lenses) in the observed core sediments implies negligible sediment transport and deposition by turbidity currents along channel floors, which is consistent with the fact that no deep-sea channels and long-lived turbidity-current channels occur along the continental margin of the northern SSIs (Fig. 1). This interpretation is supported by insignificant bottom-current erosion due to the slow and steady flow recorded in the South Shetland Trench (Nowlin and Zenk 1988), and by the reduced flow resulting from a slower Weddell Gyre during the glacials (Pudsey 1992). However, melting of the grounded ice-sheet front in contact with relatively warm water (Upper Circumpolar Deep Water) could generate sediment-laden meltwater plumes (Pudsey and Camerlenghi 1998). Such plumes may thus have reached the core site, as it is located in proximity to the continental rise (Larter and Barker 1991; Bentley and Anderson 1998).

According to Lucchi et al. (2002), the G transition facies is characterized by structureless mud with very little IRD. In core GC98-06, there is a sharp boundary between units III (G transition) and IV (Fig. 2). This may imply that G transitional sediments represent the rapid deposition of terrigenous sediments. The G transitional sediment was thus possibly deposited by the lateral spillout of low-density turbid plumes released from the advancing glaciers.

Paleoceanographic interpretation

The fossil diatom evidence, and the analyzed proxies of core GC98-06 enable us to discuss the paleoenvironmental conditions prevailing since MIS 5. In the core, MIS 5 is identified by slightly elevated TOC contents, high Ba_{bio} contents, and a high relative dominance of the ACC-associated species *T. lentiginosa*, all of which imply warmer and open-water conditions, today more prevalent in the southern Drake Passage. Although the isotopic substages (MISs 5a to 5e) cannot be distinguished by the multi-proxies in unit IV, very high TOC/Ba_{bio} values and the dominance of open-water diatoms at 196 cm core depth may be assigned to substage 5e of MIS 5. Nürnberg et al. (1997) suggested that MIS 5 may have been a time of high production south of the present Polar Front. The high

abundance of open-water taxa during MIS 5 (Fig. 5) implies a southward transport of open-water diatoms from the region north of the Polar Front of that time (Gouretski and Danilov 1994). The present Polar Front is situated 200~250 km north of the core GC98-06 site (Fig. 1), but during MIS 5 the Polar Front lay much closer to the Antarctic Peninsula margin (Pudsey 2000). As recorded by the paleoproductivity proxies uranium, Ba_{bio}, and TOC contents in the present study, higher production during MIS 5 (compared to the glacials) shows an inverse pattern to the changes in production north of the Polar Front (Rosenthal et al. 1995). This suggests that the position of the then Polar Front was located north of the core site.

In general, MISs 2 to 4 cannot be identified by multi-proxy indicators in the western Antarctic Peninsula region. However, the slightly enhanced TOC contents and lower MS values between 69 cm and 88 cm, together with high Ba_{bio} values, point to the MIS 3 period when the ocean was warmer compared to MISs 2 and 4, but colder than the Holocene and MIS 5. Cores recovered from the central part of the Drake Passage (Bae et al. 2002) suggest that increased upwelling of warmer Circumpolar Deep Water resulted in basal melting of ice shelves, with more meltwater discharge during MIS 3. MIS 2 (last glacial maximum), in turn, represents the peak of the last climatic cooling and glacial ice advance in Antarctica (Adamson and Pickard 1986). Lowest abundances of diatom valves and sea-ice taxa, together with strongly depleted Ba_{bio} levels (<100 ppm) recorded in the present study, probably imply an extension of the summer sea-ice cover to the core position, suggesting a northward shift in the Polar Front. In addition, the stronger flow of Antarctic circumpolar deep water during the glacials, compared to the interglacials (Howe and Pudsey 1999; Maldonado et al. 2006), is consistent with the presence of reworked extinct diatoms. During glacial with increased sea-ice cover, lower TOC and highly depleted Ba_{bio} of unit II are also considered to have resulted from highly reduced primary production.

The MIS 2/1 transition (base of unit I) is not clearly recorded in core GC98-06. However, the boundary extends over a distance of a few cm only, and shows an upward increase in Ba_{bio}, TOC, and trace elements associated with an upward decrease in MS values. This suggests a rapid transition, as would be expected of rapid deglaciation of the ice shelf, and a decrease in annual sea-ice cover. The IG transition facies is characterized by structureless mud containing frequent IRD layers. The IRD layers signify events of iceberg discharge from a disintegrating glacier front produced by the lift-off of grounded glaciers (Lucchi et al. 2002). A possible explanation for the poor representation of the IG transition in the core is that the grounded ice was confined to the middle shelf of the South Shetland Islands (Bentley and Anderson 1998). During the Holocene, the core site on the continental rise of the southern Drake Passage shows enrichments of trace elements coherent with proxies for productivity. The abrupt increase in TOC at the unit I/II contact, and the strong enrichment in Cd, Ni, and Zn are probably the result of abrupt glacier melting associated with meltwater pulse 1a in the northern Antarctic Peninsula (Heroy and Anderson 2007).

Conclusions

Core GC98-06 from the southern Drake Passage provides a link between local conditions in the western Antarctic Peninsula/South Shetland Islands region and regional–global climate events in the course of the last 150,000 years. Sedimentological, geochemical, and micropaleontological investigations enabled the identification of glacial, interglacial, and transitional facies associated with two major depositional processes in a continental rise setting:

1. interglacial open-marine sedimentation: the increase of open-sea diatom taxa during interglacial stages is indicative of open-marine conditions with seasonal sea-ice cover;
2. glacially derived sedimentation: a high abundance of sea-ice diatoms is representative of glacial stages, indicating an extended sea-ice cover and a grounded ice shelf.

A succession of three paleoclimatic stages is proposed to explain the sedimentary sequence of core GC98-06:

1. interglacial conditions are characterized by pervasive bioturbation with low sediment input by meltwater plumes;
2. glacial conditions are represented by indistinct facies due to the absence of mass-wasting processes (sediment slides, sediment slumps, or debris flows), resulting from the gentle topography and the South Shetland Trench; highly reduced primary production during MIS 2 was related to the presence of regionally extensive sea ice associated with an increased summer sea-ice cover at the core site;
3. the G transition represents the onset of glaciation, indicated by rapid deposition from turbid plumes.

Acknowledgements We would like to thank C.Y. Kang, M.H. Park, and S.Y. Im for their efforts during the 98/99 KARP (Korea Antarctic Research Program) cruise to the Drake Passage. We are also grateful to the crew of the R/V *Yuzhmorgeologiya* for all their assistance with gravity coring. Finally, we acknowledge the constructive comments of Prof. F.J. Hernández Molina, Dr. M.T. Delafontaine, and an anonymous reviewer that helped to improve the paper. This research was funded by KOPRI Grant PE09010.

References

Adamson DA, Pickard J (1986) Cainozoic history of the Vestfold Hills. In: Pickard J (ed) Antarctic oasis. Terrestrial environments and history of the Vestfold Hills. Academic, Sydney, pp 63–93

Bae SH, Yoon HI, Park B-K, Kang CY (2002) Stable isotope record and depositional environments in the Antarctic Polar Front of Drake Passage, Western Antarctica. Geosci J 6(2):117–123

Bae SH, Yoon HI, Park B-K, Kim Y (2003) Late Quaternary stable isotope record and meltwater discharge anomaly events to the south of the Antarctic Polar Front, Drake Passage. Geo-Mar Lett 23(2):110–116. doi:10.1007/s00367-003-0129-y

Bak Y-S, Lee J-D, Yoon HI, Yun H, Kim H-J (2002) Quaternary diatom assemblages from sediment core GC 98–06 in the southern Drake Passage, Antarctica (in Korean with English abstract). J Korean Earth Sci Soc 23(5):442–453

Baldauf JG, Barron JA (1991) Diatom biostratigraphy: Kerguelen Plateau and Prydz Bay regions of the southern ocean. In: Barron JA, Larsen B, Baldauf JG et al. (eds) Proc Ocean Drilling Program, Sci Results 119:547–598

Barker PF, Camerlenghi A, Acton GD et al. (1999) Initial results of the Ocean Drilling Program, Leg 178. College Station, TX, http://www-odp.tamu.edu/publications/178_IR/178TOC.HTM

Battarbee R (1973) A new method for estimating absolute microfossil number with special reference to diatoms. Limnol Oceanogr 18:647–653

Bentley MJ, Anderson JB (1998) Glacial and marine geological evidence for the ice sheet configuration in the Weddell Sea-Antarctic Peninsula region during the Last Glacial Maximum. Antarctic Sci 10:309–325

Berkman PA, Andrew JT, Bjorck S, Colhoun EA, Emslis S, Goodwin ID, Hall BL, Hart CP, Hirakawa K, Igarashi A, Ingolfson O, Lopez-Martinez J, Lyons WB, Mabin MCG, Quilty PG, Taviani M, Yoshida Y (1998) Circum-Antarctic coastal environmental shifts during the Late Quaternary reflected by emerged marine deposits. Antarctic Sci 10:345–362

Bonn WJ (1995) Biogenic opal and barium: indicators for late Quaternary changes in productivity at the Antarctic continental margin, Atlantic sector. Ber Polarforsch 180:1–186

Carmack EC (1977) Water characteristics of the Southern Ocean south of the Polar Front. In: Angel M (ed) A voyage of discovery, George Deacon 70th anniversary volume. Pergamon, Oxford, pp 15–41

Ciesielski PF (1983) The Neogene and Quaternary diatom biostratigraphy of subantarctic sediments, Deep Sea Drilling Project Leg 71. In: Ludwig WJ, Krasheninnikov VA (eds), Initial Rep Deep Sea Drilling Project, 71:635–665

Domack EW, Williams CR (1990) Fine structure and suspended sediment transport in three Antarctic fjords. Contrib Antarct Res 50:71–89

Domack E, Leventer A, Dumbar R, Taylor F, Brachfeld S, Sjunneskog C, ODP Leg 178 Scientific Party (2001) Chronology of the Palmer Deep site, Antarctic Peninsula: a Holocene paleoenvironmental reference for the circum-Antarctic. Holocene 11:1–9

Foldvik A, Gammelsrød T (1988) Notes on Southern Ocean hydrography, sea-ice and bottom water formation. Palaeogeogr Palaeoclimatol Palaeoecol 67:3–17

Folk RL, Ward WC (1957) Brazos river bars. A study in the significance of grain size parameters. J Sediment Petrol 27:3–26

Ganachaud A, Wunsch C (2000) Improved estimates of global ocean circulation, heat transport and mixing from hydrographic data. Nature 408:453–457

Gersonde R, Barcena MA (1998) Revision of the upper Pliocene-Pleistocene diatom biostratigraphy for the normative belt of the Southern Ocean. Micropaleontology 44:84–98

Gouretski VV, Danilov AI (1994) Characteristics of warm rings in the African sector of the Antarctic Circumpolar Current. Deep-Sea Res 41:1131–1157

Griffith W, Anderson JB (1989) Climatic control of sedimentation in bays and fjords of the northern Antarctic Peninsula. Mar Geol 85:181–204

Harden SL, DeMaster DJ, Nittrouer CA (1992) Developing sediment geochronologies for high-latitude continental shelf deposits: a radiochemical approach. Mar Geol 103:69–97

Hernández-Molina FJ, Larter RD, Rebesco M, Maldonado A (2006) Miocene reversal of bottom water flow along the Pacific Margin of the Antarctic Peninsula: stratigraphic evidence from a contourite sedimentary tail. Mar Geol 228:93–116

Heroy DC, Anderson JB (2007) Radiocarbon constraints on Antarctic Peninsula Ice Sheet retreat following the Last Glacial Maximum (LGM). Quat Sci Rev 26:3286–3297

Hesse R, Khodabakhsh S, Klauck I, Ryan WBF (1997) Asymmetrical turbid surface-plume deposition near ice-outlets of the Pleistocene Laurentide ice sheet in the Labrador Sea. Geo-Mar Lett 17:179–187. doi:10.1007/s003670050024

Hesse R, Klauck I, Khodabakhsh S, Piper D (1999) Continental slope sedimentation adjacent to an ice margin. III. The upper Labrador Slope. Mar Geol 155:249–276

Howe JA, Pudsey CJ (1999) Antarctic circumpolar deep water: a Quaternary paleoflow record from the northern Scotia Sea, South Atlantic Ocean. J Sediment Res 69(4):847–861

Jones KPN, McCave IN, Patel PD (1988) A computer-interfaced sedigraph for modal size analysis of fine-grained sediment. Sedimentology 35:163–172

Kim Y, Kim HS, Larter RD, Camerlenghi A, Gambôa LAP, Rudowski S (1995) Tectonic deformation in the upper crust and sediments at the South Shetland Trench. Antarct Res Ser 68:157–166

Klepeis KA, Lawver LA (1996) Tectonics of the Antarctic-Scotia plate boundary near Elephant and Clarence Islands, West Antarctica. J Geophys Res 101:20211–20231

Larter RD, Barker PF (1991) Neogene interaction of tectonic and glacial processes at the Pacific margin of the Antarctic Peninsula. In: MacDonald DIM (ed) Sedimentation, tectonics and eustasy. IAS Spec Publ 12:165–186

Lucchi RG, Rebesco M, Camerlenghi A, Busetti M, Tomadin L, Villa G, Persico D, Morigi C, Bonci MC, Giorgetti G (2002) Mid-late Pleistocene glacimarine sedimentary processes of a high-latitude, deep-sea sediment drift. Mar Geol 189:343–370

Maldonado A, Bohoyo F, Galindo-Zaldívar J, Hernández-Molina J, Jabaloy A, Lobo FJ, Rodríguez-Fernández J, Suriñach E, Vázquez JT (2006) Ocean basins near the Scotia-Antarctic plate boundary: influence of tectonics and paleoceanography on the Cenozoic deposits. Mar Geophys Res 27(2):83–107

Naveira Garabato AC, Heywood KJ, Stevens DP (2002a) Modification and pathways of Southern Ocean Deep Waters in the Scotia Sea. Deep-Sea Res I 49:681–705

Naveira Garabato AC, McDonagh EL, Stevens DP, Heywood KJ, Sanders RJ (2002b) On the export of Antarctic Bottom Water from the Weddell Sea. Deep-Sea Res II 49:4715–4742

Nowlin WD, Zenk W (1988) Westward bottom currents along the margin of the South Shetland Island Arc. Deep-Sea Res 35:269–301

Nürnberg CC, Bohrmann G, Schluter M, Frank M (1997) Barium accumulation in the Atlantic sector of the Southern Ocean: results from 190, 000-year records. Paleoceanography 12:594–603

Orsi AH, Whitworth T III, Nowlin WD Jr (1995) On the meridional extent and fronts of the Antarctic Circumpolar Current. Deep-Sea Res 42:641–673

Orsi AH, Johnson GC, Bullister JL (1999) Circulation, mixing and production of Antarctic Bottom Water. Progr Oceanogr 43:55–109

Pelayo AM, Wiens DA (1989) Seismotectonics and relative plate motions in the Scotia Sea region. J Geophys Res 94(B6):7293–7320

Pudsey CJ (1992) Late Quaternary changes in Antarctic Bottom Water velocity inferred from sediment grain size in the northern Weddell Sea. Mar Geol 107:9–33

Pudsey CJ (2000) Sedimentation on the continental rise west of the Antarctic Peninsula over the last three glacial cycles. Mar Geol 167:313–338

Pudsey CJ, Camerlenghi A (1998) Glacial-interglacial deposition on a sediment drift on the Pacific margin of the Antarctic Peninsula. Antarctic Sci 10:286–308

Pudsey CJ, Howe JA (1998) Quaternary history of the Antarctic Circumpolar Current: evidence from the Scotia Sea. Mar Geol 148:83–112

Quayle WC, Peck LS, Peat H, Ellis-Evans JC, Harrigan PR (2002) Extreme responses to climate change in Antarctic lakes. Science 295:645

Rosenthal Y, Boyle EA, Labeyrie L, Oppo D (1995) Glacial enrichments of authigenic Cd and U in Subantarctic sediments: a climatic control on the elements' oceanic budget? Paleoceanography 10:395–413

Vaughan DG, Marshall GJ, Connolley WM, King JC, Mulvaney R (2001) Devil in the detail. Science 293:1777–1779

Yoon HI, Park B-K, Kim Y, Kang CY (2002) Glaciomarine sedimentation and its paleoclimatic implications on the Antarctic Peninsula shelf over the last 15000 years. Palaeogeogr Palaeoclimatol Palaeoecol 185:235–254